

Supplementary Information

Bio-inspired Proton Relay for Promoting Continuous 5-Hydroxymethylfurfural Electrooxidation in Flowing System

Dexin Chen^{1,2†}, Wenlong Li^{1,2†}, Junbo Liu^{1,2} and Licheng Sun^{1,2*}

¹*School of Materials Science and Engineering, Zhejiang University, Hangzhou 310027, Zhejiang Province, China.*

²*Center of Artificial Photosynthesis for Solar Fuels and Department of Chemistry, School of Science and Research Center for Industries of the Future, Westlake University, Hangzhou 310030, Zhejiang Province, China.*

³*Division of Solar Energy Conversion and Catalysis at Westlake University, Zhejiang Baima Lake Laboratory Co., Ltd., Hangzhou 310000, Zhejiang Province, China.*

[†]*These authors contributed equally to this work.*

^{*}*Corresponding author. Email: sunlicheng@westlake.edu.cn*

1. EXPERIMENTAL SECTION

Section S1: Synthesis of electrocatalysts

Chemical reagents. Commercial Ni foam was purchased from Suzhou Xingzhenghong Technology Co., Ltd. Hydrochloric acid (AR), sulfuric acid (AR), KOH (AR), NaOH (AR), $\text{Ni}(\text{NO}_3)_2 \cdot 6\text{H}_2\text{O}$ (AR), terephthalic acid (AR), sodium terephthalate (AR), urea (AR), and NH_4F (AR) were purchased from the Aladdin company. Ethanol, isopropanol, N,N-dimethylformamide (DMF), 5-hydroxymethylfurfural (HMF, 99%), and 2,5-furandicarboxylic acid (FDCA, 99.5%) were purchased from Adamas company. 5-hydroxymethylfurancarboxylic acid (HMFCFA, 98%), 2,5-diformylfuran (DFF, 98%), and 2,5-furandicarboxylic acid (FDCA, 98%) were purchased from Alfa Aesar. D_2O (99.8 atom%D) is purchased from JKchemical and NaOD (40%) is purchased from Cambridge Isotope Laboratories. The ultrapure water was obtained by Milli-Q (Millipore, $18.2 \text{ M}\Omega \text{ cm}^{-1}$).

Synthesis of $\text{Ni}(\text{OH})_2$. A piece of Ni foam (1 mm thickness, $2.2 \times 2.5 \text{ cm}^2$) was cut and washed in 3 M HCl for 20 min, followed by ultrasonication in ethanol and acetone for 20 min, respectively. Then, Ni foam was placed in an aqueous solution (30 ml) which consists of 1 mmol $\text{Ni}(\text{NO}_3)_2 \cdot 6\text{H}_2\text{O}$, 6 mmol urea, and 4 mmol NH_4F . The above solution was transferred to a Teflon-lined autoclave and kept at 120°C for 8 hours. When the temperature dropped to room temperature, the catalyst was taken out, and washed with deionized water (DI water) and ethanol three times, respectively. Then, it was dried under vacuum, and denoted as $\text{Ni}(\text{OH})_2$.

Synthesis of $\text{Ni}(\text{OH})_2$ -TPA. $\text{Ni}(\text{OH})_2$ was placed in a Teflon-lined autoclave consisting of 0.75 mmol terephthalic acid, 27 ml DMF, and 3 ml H_2O . Then, the autoclave was heated up to 120°C for 5 hours. When it cooled down to room temperature, the catalyst was taken out and rinsed with DI water and ethanol three times, respectively. The catalyst was dried under vacuum, and denoted as $\text{Ni}(\text{OH})_2$ -TPA.

Synthesis of Ni-Mo/NF. A piece of Ni foam (1 mm thickness, $2.2 \times 2.5 \text{ cm}^2$) was placed in an aqueous solution (30 ml) which consists of 1.6 mmol $\text{Ni}(\text{NO}_3)_2 \cdot 6\text{H}_2\text{O}$ and 0.4 mmol $(\text{NH}_4)_6\text{Mo}_7\text{O}_{24} \cdot 4\text{H}_2\text{O}$. The above solution was transferred to a Teflon-lined autoclave and kept at 150°C for 6 hours. The as-synthesized NiMoO_4 was heated at 500°C for 2 hours in a H_2/Ar (5/95) atmosphere, and the obtained catalyst was denoted as Ni-Mo/NF.

Section S2: Structure characterization and electrochemical tests

Structural characterizations. Powder X-ray diffraction (PXRD) was performed on a Bruker D8 Advance X-ray diffractometer with Cu K α (0.154 nm) radiation. Scanning electron microscopy images were obtained using ZEISS Gemini 450 field emission SEM (FESEM) with an accelerating voltage of 15 kV. Transmission electron microscopy (TEM), high-resolution TEM (HR-TEM), and EDS elemental mapping images were collected by Talos F200X G2 electron microscope with an accelerating voltage of 200 kV. X-ray photoelectron spectroscopy (XPS) was carried out on Nexsa G2 Micro-focus X-Ray Photoelectron Spectrometer (Thermo Fisher Scientific). Raman spectroscopic tests are conducted on the Alpha300RAS Raman Spectrometer (WITec) (excitation wavelength: 532 nm; number of accumulations: 20; integration time: 5 s). For the quasi-in-situ Raman test, the catalysts were first activated in corresponding solutions followed by being taken out and tested. Fourier transform infrared (FT-IR) spectrum and in situ attenuated total reflectance surface-enhanced infrared absorption spectroscopy (ATR-SEIRAS) are performed on Nicolet iS50 (Thermo FisherTM). For the ATR-SEIRAS test, the solution consisted of 1.0 M KOH and 10 mM HMF.

Electrochemical measurements. Electrochemical tests were carried out on an electrochemical workstation (Autolab-Vionic, Metrohm) in a divided H-type cell with a three-electrode configuration. The as-synthesized catalyst was used as the working electrode (WE), Hg/HgO was taken as the reference electrode (RE), and Pt mesh was used as the counter electrode (CE). The anode and cathode were separated by a Nafion 212 membrane. Both anolyte and catholyte were fed with 1.0 M KOH solution. All potentials in this work were calibrated to the reversible hydrogen electrode (RHE) by applying the following equation unless otherwise stated:

$$E_{\text{RHE}} = E_{\text{measured}} + E_{\text{Hg/HgO}} + 0.0591 \times \text{pH} \quad (1)$$

The potential of the Hg/HgO electrode was calibrated by a standard hydrogen electrode (SHE).

As mentioned, the quasi-steady state linear sweep voltammetry (QS-LSV) curve was plotted to reflect the accurate activity of the catalyst for HMF oxidation. Each point referred to the stabilized current density recorded at a certain potential from the *i*-t test.

To evaluate the reaction kinetics, Tafel slope was obtained by equation (2):

$$\eta = b \log j + a \quad (2)$$

where j denotes the current density, η refers to the overpotential, and b is the calculated Tafel slope. To obtain a more precise Tafel slope, equilibrated potentials under different current densities were recorded with a stabilization time of over 60 s and repeated three times to depict the error bar. Electrochemical double-layer capacity (C_{dl}) was carried out by CV scans in the potential range of 0~0.20 V vs. Hg/HgO with a scan rate of 20, 40, 60, 80, and 100 mV/s. The $\Delta j/2$ obtained at 0.10 V vs. Hg/HgO was plotted against the scan rate, and the fitted slope was measured as the C_{dl} value. The electrochemical surface area (ECSA) value was calculated as C_{dl}/C_s . Operando electrochemical impedance spectroscopy (EIS) was performed at a potential of 1.25~1.55 V vs. RHE with a frequency from 10 kHz to 0.1 Hz by an amplitude of 10 mV, and the sampling interval was set at 50 mV. Open-circuit potential (OCP) tests were carried out in 1.0 M KOH with and without 100 mM HMF. Before the test, the electrode was activated in the corresponding solution for 5 min under 0.50 V vs. Hg/HgO, and then the OCP value was recorded.

Section S3: Construction of HMF oxidation electrolyzer and product analysis

Construction of HMF oxidation electrolyzer. The anion exchange membrane (AEM)-based HMF oxidation electrolysis was performed on a single cell with serpentine flow fields (1 cm² and 25 cm², respectively). Ni(OH)₂-TPA was taken as the anode, and Ni-Mo/NF was taken as the cathode, and PAP-TP-85 (A40) was used as the AEM. KOH solution (2 M) and HMF solution in H₂O (400 mM) are separately placed and mixed before flowing into the reactor. For the LSV test, a scan rate of 5 mV s⁻¹ was applied, and the flow rate of electrolyte was set at 30 ml min⁻¹. For the chronopotentiometry (CP) test, a total current of 7,500 mA cm⁻² (300 mA cm⁻²) was applied with a flow rate of 3.81 ml min⁻¹.

Product analysis. The concentrations of the organics were determined by high-performance liquid chromatography (HPLC, Shimadzu 2050 C) with a wavelength of UV-Vis detector set at 265 nm. A 4.6×250 mm Shim-pack GIST 5 μm C18 column was applied. The HPLC eluent consisted of 70% (v/v) 5 mM ammonium formate solution and 30% (v/v) methanol and was performed at a flow rate of 0.59 mL min⁻¹ for 10 min (column temperature: 40 °C). The HPLC samples were prepared by diluting 10 μL electrolyte to 2.5 mL by H₂O. For stability measurement, the total volume of the anolyte is 10 mL fed with 100 mM HMF. The Faradaic efficiency (FE) and yield of FDCA were calculated by the following equations:

$$\text{Faradaic efficiency (\%)} = n_{\text{experimentally formed}} / (Q / (6 \times F)) \times 100\% \quad (3)$$

$$\text{Yield (\%)} = n_{\text{experimentally formed}} / n_{\text{theoretically formed}} \times 100\% \quad (4)$$

$$\text{Carbon balance (\%)} = n_{\text{all organics}} / n_{\text{HMF input}} \times 100\% \quad (5)$$

where n is the mole number of the substrate formed experimentally and theoretically. Q is the charge transferred over the reaction, and F refers to Faraday's constant ($96,485 \text{ C mol}^{-1}$).

Section S4: Techno-economic analyses (TEA)

For an industrial-related scenario, the production of FDCA can be assumed to be $1,000 \text{ kg day}^{-1}$.

The yield of FDCA is assumed to be 99%,

$$\begin{aligned} 1. \quad \text{HMF}_{\text{input}} &= 1,000 \text{ kg}_{\text{FDCA}} \text{ day}^{-1} \div M_{\text{FDCA}} \times M_{\text{HMF}} \div \text{Yield} \\ &= 1,000 \text{ kg}_{\text{FDCA}} \text{ day}^{-1} \div 156 \times 126 \div 99\% = 816 \text{ kg day}^{-1} \end{aligned}$$

The Faradaic efficiency of FDCA is assumed to be 98%,

2. Total current = $816 \text{ kg day}^{-1} \times 10^3 \div 126 \times 6 \times 96,485 \div (24 \times 3,600) \div 98\% = 44,278 \text{ A day}^{-1}$
3. Power = $UI = 1.7 \text{ V} \times 44,278 \text{ A day}^{-1} \times 10^{-3} = 75.27 \text{ kW day}^{-1}$
4. Electricity cost = $75.27 \text{ kW} \times 24 \text{ h} \times X \text{ CNY/kWh} = 1806.5 X \text{ CNY day}^{-1}$ (X refers to the electricity price)
5. Electrolyzer area = $44,278/y \text{ cm}^2$ here, y refers to the current density (A cm^{-2})
6. H_2 produced = $44,278 \times 24 \times 3,600 \times 2 \times 10^{-3} \div (2 \times 96,485) = 39.65 \text{ kg day}^{-1}$

In this work, the electrolyte consists of 1.0 M KOH and 200 mM HMF,

$$7. \quad \text{Mass of HMF needed in 1.0 L H}_2\text{O} = 1.0 \text{ L} \times 0.2 \text{ mol L}^{-1} \times 126 \text{ g mol}^{-1} = 25.2 \text{ g}$$

H_2O price = 3 CNY tonne^{-1} , KOH price = 5.8 CNY kg^{-1} , H_2SO_4 price = 0.26 CNY kg^{-1} . Ideally, the HMF price is assumed to be 10 CNY kg^{-1} for academic analysis, which is a competitive price for PET.

8. HMF cost = $816 \times 10 = 8,160 \text{ CNY day}^{-1}$
9. H_2O consumption = $816 \times 1,000 \div 25.2 = 32,381 \text{ L day}^{-1}$
10. H_2O cost = $32,381 \times 10^{-3} \times 3 = 97.1 \text{ CNY day}^{-1}$

11. KOH consumption = $32,381 \times 1.0 \times 56 \times 10^{-3} = 1813.3 \text{ kg day}^{-1}$
12. KOH cost = $1813.3 \text{ kg day}^{-1} \times 5.8 = 10,517.1 \text{ CNY day}^{-1}$
13. H₂SO₄ consumption = $32,381 \times 0.5 \times 98 \times 10^{-3} = 1,586.7 \text{ kg day}^{-1}$
14. H₂SO₄ cost = $1,586.7 \text{ kg day}^{-1} \times 0.26 = 412.5 \text{ CNY day}^{-1}$

Calculation of the fixed cost

Ni plate price = 300 CNY kg⁻¹, PEEK price = 800 CNY kg⁻¹, Silicon rubber price = 30 CNY kg⁻¹,
GDL price (Ni foam, 1.0 mm thickness) = 400 CNY m⁻²

15. Unit electrolyzer cost (including the connector) = 8.0 CNY cm⁻²

The electrolyzer is assumed to run for 5 years (running 350 days year⁻¹).

16. Electrolyzer stack cost = $44,278/\text{y} \times 8.0 / (5 \times 350) = 202.4/\text{y} \text{ CNY day}^{-1}$

Electrolyzer maintenance is assumed to be 2.5% of the total stack cost.

17. Electrolyzer maintenance cost = $202.4/\text{y} \times 2.5\% = 5.1/\text{y} \text{ CNY day}^{-1}$

The Balance of Plant (BOP) is set as 50% of the electrolyzer stack cost.

18. BOP = $202.4/\text{y} \times 50\% = 101.2/\text{y} \text{ CNY day}^{-1}$

Separation capital cost is assumed to be 30% of electrolyzer stack cost.

19. Separation capital cost = $202.4/\text{y} \times 30\% = 60.7/\text{y} \text{ CNY day}^{-1}$

The total cost of electrocatalysts and membrane (MEA) is 3% of the electrolyzer stack cost.

20. MEA cost = $202.4/\text{y} \times 3\% = 6.1/\text{y} \text{ CNY day}^{-1}$

$$\begin{aligned}
 \text{Total cost of FDCA per day} &= \text{Electricity cost} + \text{HMF cost} + \text{H}_2\text{O cost} + \text{KOH cost} + \text{H}_2\text{SO}_4 \text{ cost} \\
 &+ \text{Electrolyzer stack cost} + \text{Maintenance cost} + \text{BOP cost} + \text{Separation capital cost} + \text{MEA cost} \\
 &= 1806.5 X + 8,160 + 97.1 + 10517.1 + 412.5 + 202.4/\text{y} + 5.1/\text{y} + 101.2/\text{y} + 60.7/\text{y} + 6.1/\text{y} \\
 &= 1806.5 X + 19,186.6 + 375.5/\text{y} \tag{6}
 \end{aligned}$$

Based on this equation, the phase diagram of FDCA cost against the electricity price and current density (of the electrolyzer) can be plotted. To study the influence of FDCA price by different HMF concentrations, the electrolytes consisting of 1.0 M KOH fed with 400 mM HMF and 100

mM HMF are investigated accordingly, and the total cost of FDCA is calculated as equations (7) and (8):

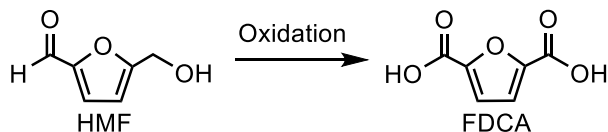
$$\begin{aligned} \text{Total cost of FDCA (400 mM HMF)} &= 1806.5 X + 8160 + 48.6 + 5258.7 + 206.3 + 375.5/y \\ &= 1806.5 X + 13673.6 + 375.5/y \end{aligned} \quad (7)$$

$$\begin{aligned} \text{Total cost of FDCA (100 mM HMF)} &= 1806.5 X + 8160 + 194.3 + 21034.3 + 825.1 + 375.5/y \\ &= 1806.5 X + 30213.7 + 375.5/y \end{aligned} \quad (8)$$

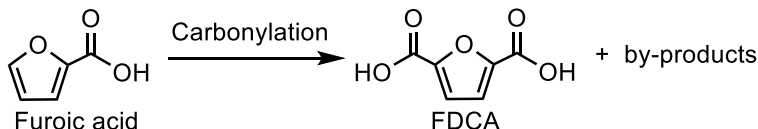
Note S1

there are several existing strategies for FDCA production, including the following main routes:

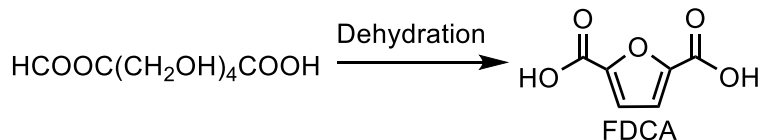
1. **HMF-based route.** HMF, derived from cellulose, glucose, and fructose, can be directly oxidized to FDCA, which exhibits great potential for industrialization.



2. **Furoic acid-based route.** FDCA can also be obtained by carbonylation of furoic acid. But this route would bring some by-products and exhibit a low yield of FDCA.



3. **Hexaric acid-based route.** The hexaric acids including glucaric acid and galactaric acid, derived from glucose and lactose, can be used as starting materials for FDCA production through the dehydration process. However, the reactants are prone to isomerization and carbonization, which would cause low yields of FDCA.



4. **Other routes** using diglycolic acid, mucic acid, and 2,5-dimethylfuran as starting materials can also be applied for FDCA production.

In the above routes, the **HMF-based route** is most widely applied for FDCA production. The HMF oxidation system to produce FDCA mainly includes chemical oxidation, thermocatalysis, electrocatalysis, and enzymatic catalysis. Among them, electrocatalysis, particularly AEM-based HMF electrooxidation for FDCA production is an emerging sustainable technology, which features the following advantages:

1. **Benign reaction conditions.** AEM-HMFOR requires mild reaction conditions, which can be operated below 40°C under ambient air in this work. Water (H₂O) is used as the green oxygen source and chemical oxidants are needless in this system.
2. **High FDCA yield and selectivity.** FDCA obtained through electrocatalysis in this work exhibits a high yield of over 99% and selectivity of nearly 100%, which helps lower the subsequent separation and purification cost.
3. **Couple with renewable electricity.** AEM-HMFOR system can be coupled with green hydrogen production using renewable electricity (wind, solar energy, etc.) to further decrease the production cost of FDCA and reduce carbon emission.

Commercial FDCA production generally utilizes thermocatalysis and chemical oxidation. Based on the existing mature chemical industry chain, those approaches exhibit advantages in scale-up production. Thus, developing highly efficient electrocatalysts and catalytic systems shows great significance in accelerating FDCA production through electrocatalysis.

3. SUPPLEMENTARY FIGURES

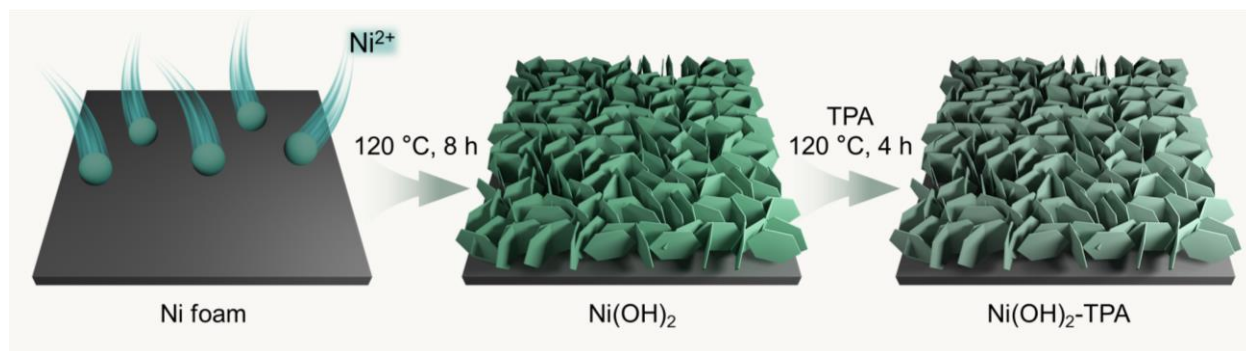


Fig. S1. Synthesis of Ni(OH)₂-TPA via a two-step hydrothermal method.

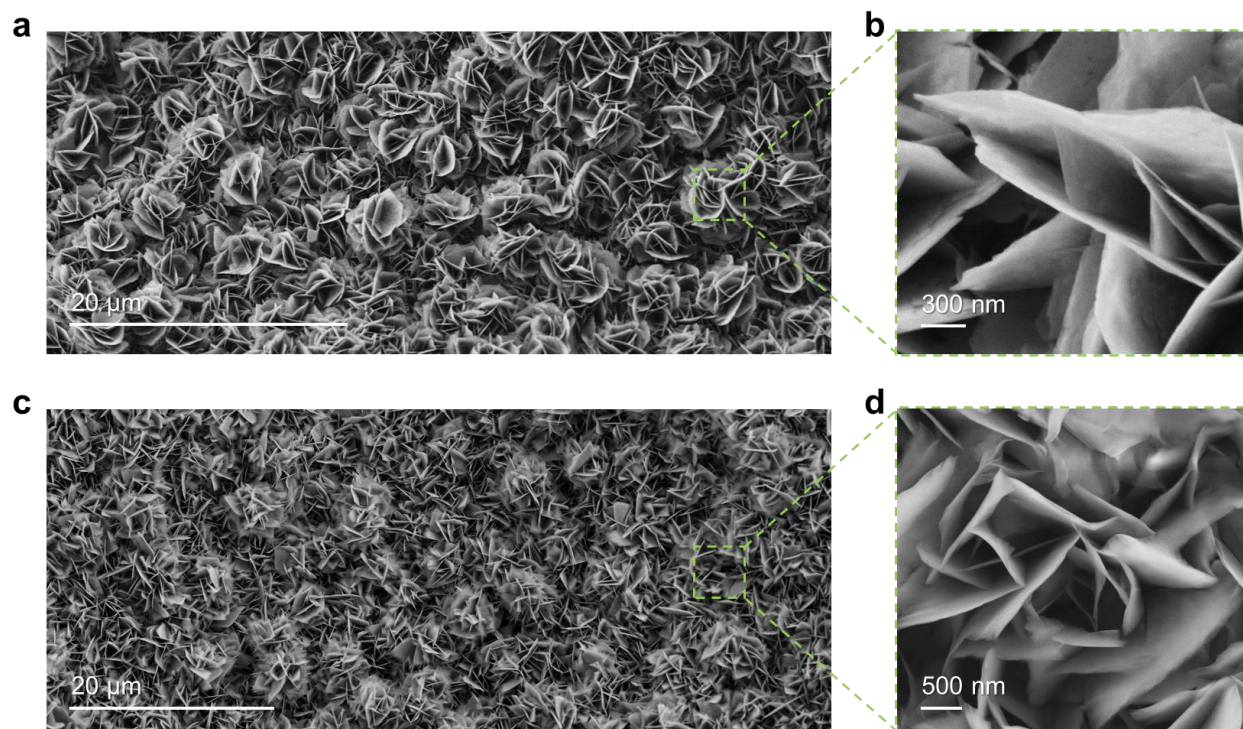


Fig. S2. FE-SEM images of (a)-(b) Ni(OH)₂ and (c)-(d) Ni(OH)₂-TPA with different magnifications. Both Ni(OH)₂ and Ni(OH)₂-TPA are evenly dispersed on Ni foam.

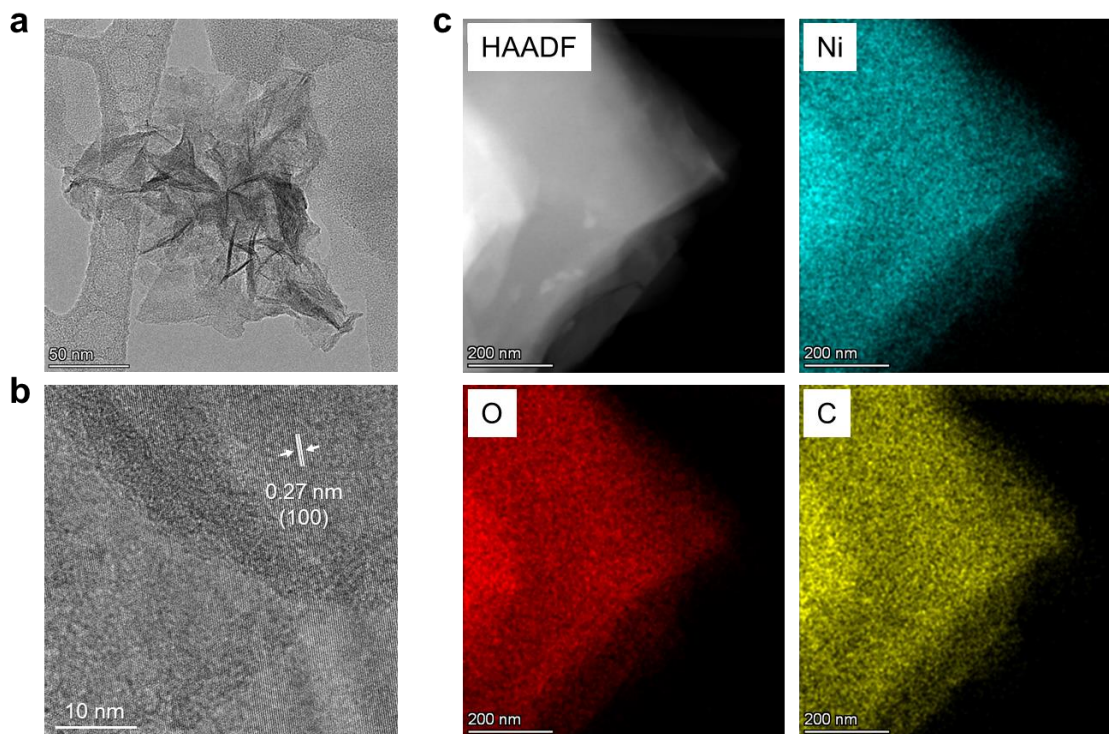


Fig. S3. (a)-(b) Transmission electron microscopy (TEM) images of Ni(OH)₂-TPA with different magnifications. (c) element dispersive spectrometer analysis. Ni, O, and C elements are evenly distributed.

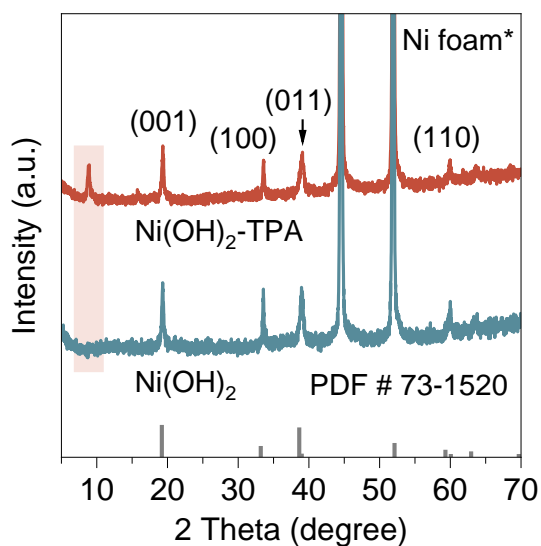


Fig. S4. XRD patterns of Ni(OH)₂-TPA and Ni(OH)₂.

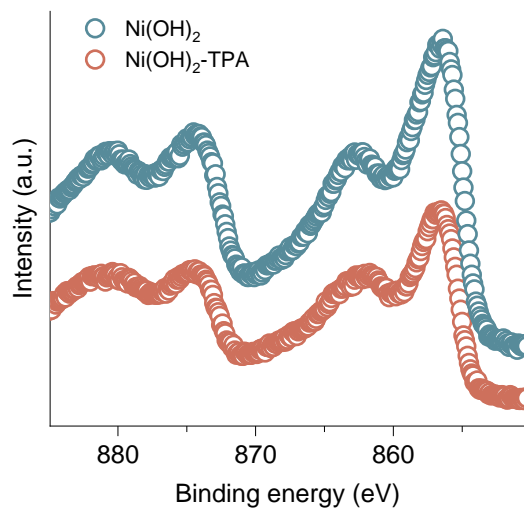


Fig. S5. High-resolution X-ray photoelectron spectroscopy (XPS) spectrum of Ni(OH)_2 and $\text{Ni(OH)}_2\text{-TPA}$.

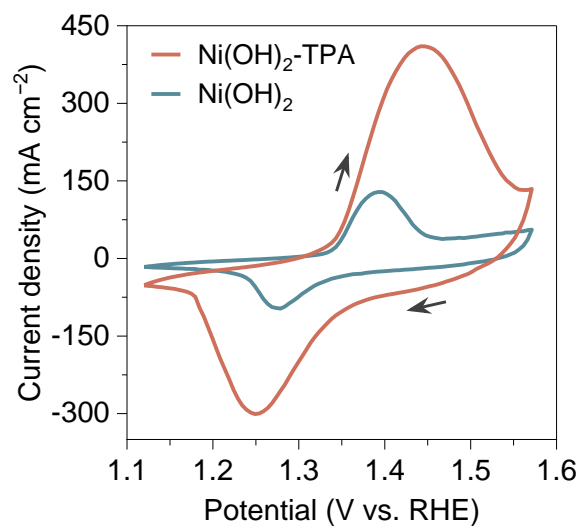


Fig. S6. Investigation on redox properties of catalysts. CV scans (50 mV s^{-1}) of $\text{Ni(OH)}_2\text{-TPA}$ and Ni(OH)_2 in 1.0 M KOH solution. The black arrows refer to the scan direction.

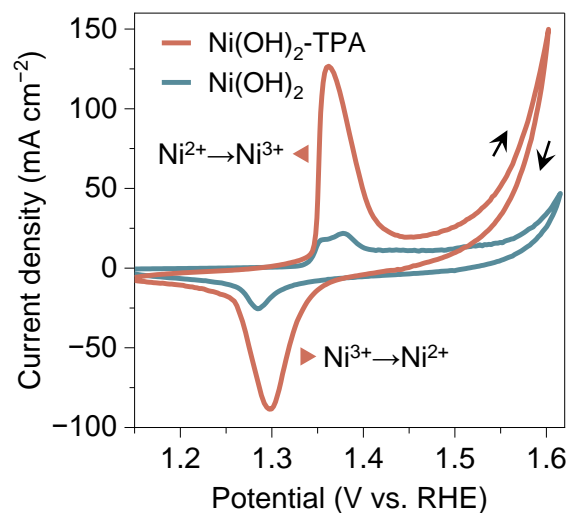


Fig. S7. Investigation on OER performances. CV plots (5 mV s^{-1}) of $\text{Ni(OH)}_2\text{-TPA}$ and Ni(OH)_2 in 1.0 M KOH solution. The black arrows refer to the scan direction.

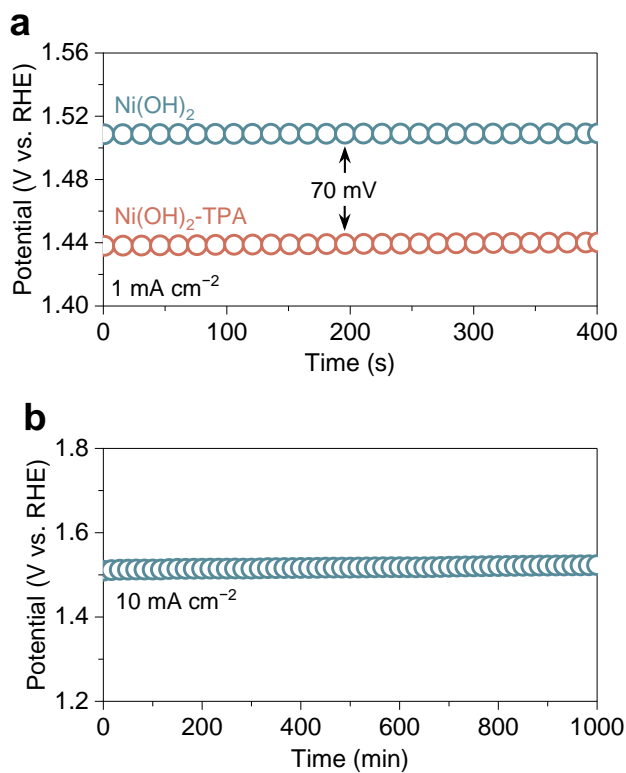


Fig. S8. (a) Determination of onset potential through CP tests at a current density of 1 mA cm^{-2} . **(b)** CP test of $\text{Ni(OH)}_2\text{-TPA}$ at 10 mA cm^{-2} in 1.0 M KOH solution.

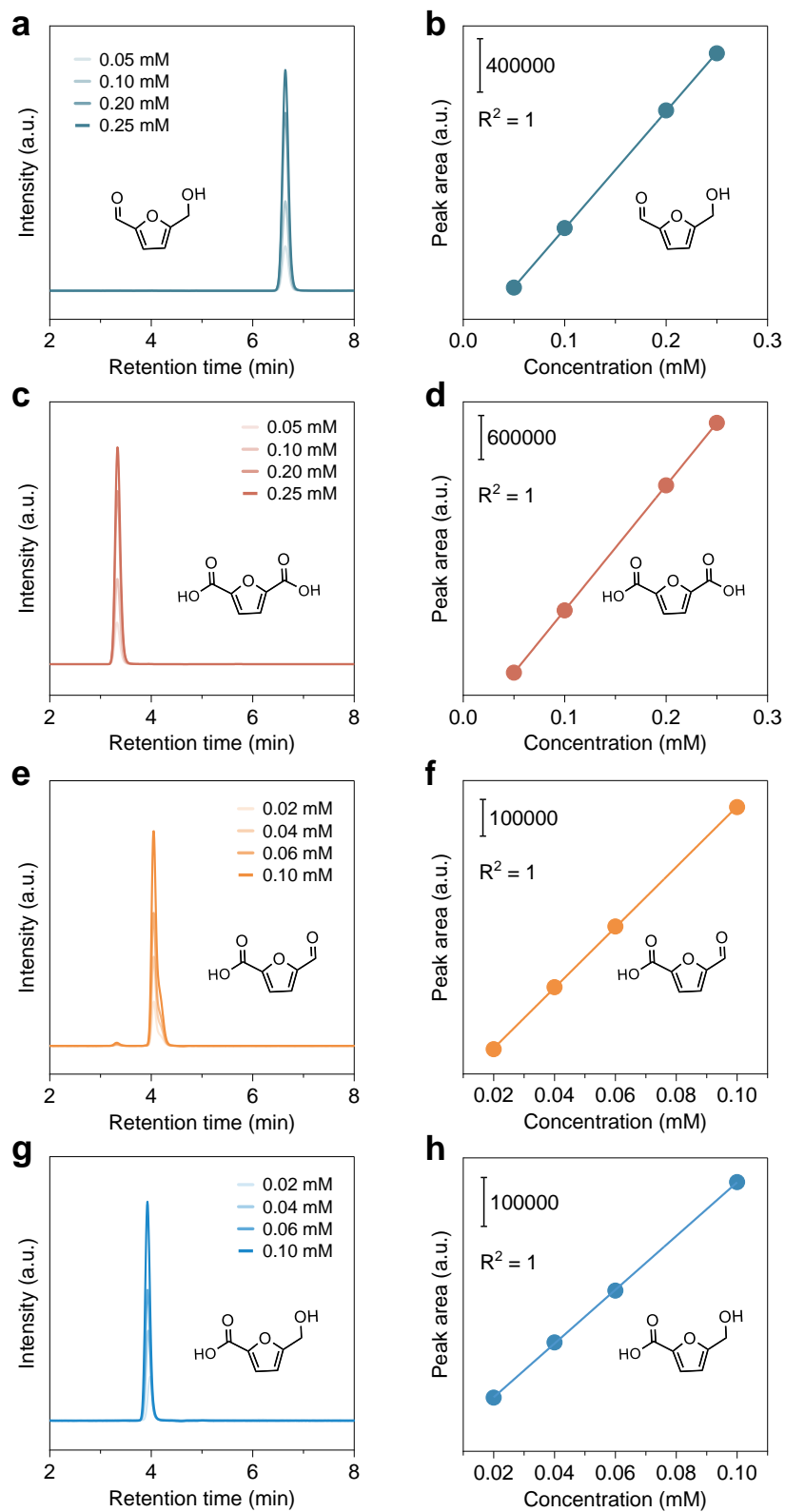


Fig. S9. HPLC analysis. HPLC chromatograms and corresponding standard curves for (a)-(b) HMF, (c)-(d) FDCA, (e)-(f) FFCA, and (g)-(h) HMFCA with different concentrations.

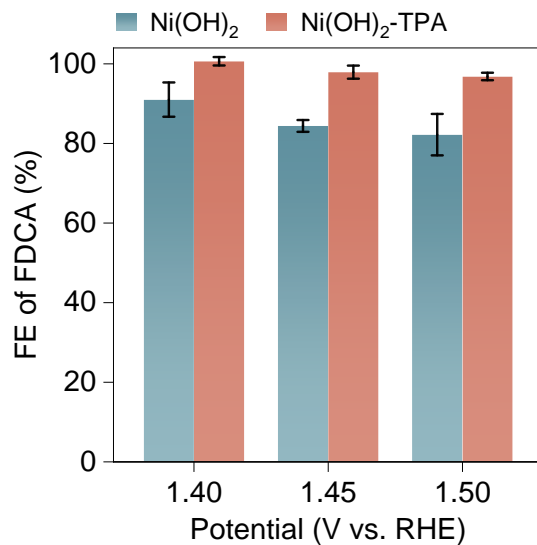


Fig. S10. FEs of FDCA with elevating potentials in the presence of 100 mM HMF.

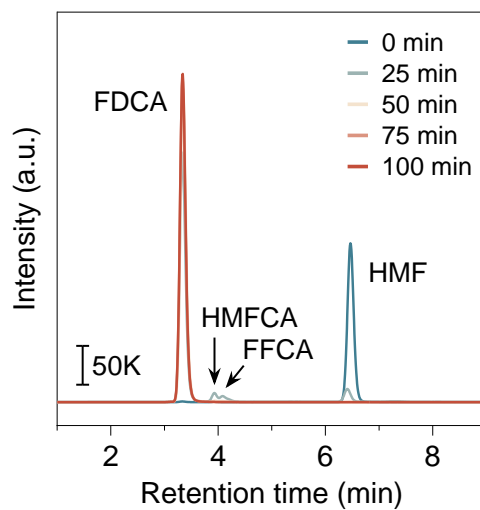


Fig. S11. The evolution of organic compounds within 100 min in the presence of 100 mM HMF.

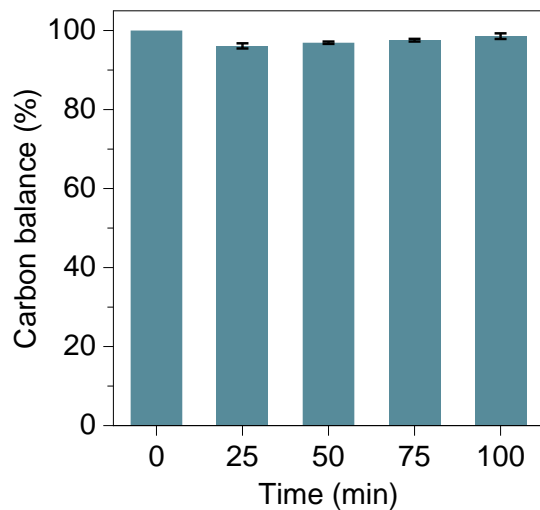


Fig. S12. Evolution of carbon balance in the presence of 100 mM HMF. The carbon balance is measured to be nearly 100%, demonstrating the rapid HMF oxidation rate and negligible HMF degradation in the KOH solution.

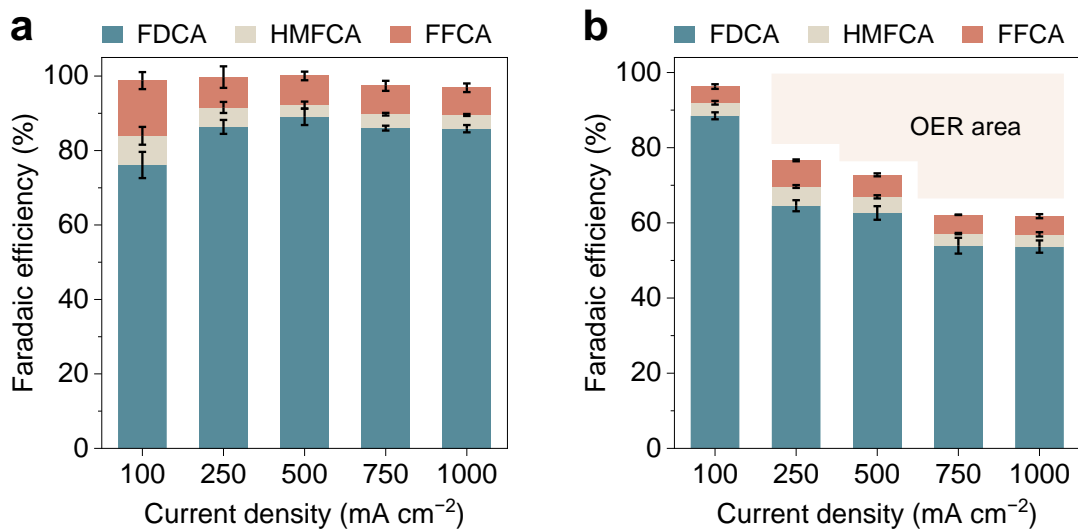


Fig. S13. The evolution of FEs of oxidation products (FDCA, HMFCa, and FFCA) with elevating current densities for (a) Ni(OH)₂-TPA and (b) Ni(OH)₂ with 100 mM HMF. The charge passed through the electrode is controlled to be 100 C.

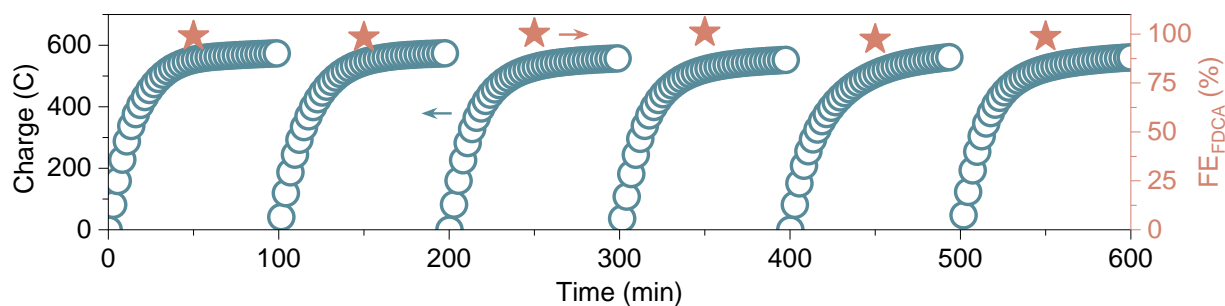


Fig. S14. Stability evaluation of Ni(OH)₂-TPA with 100 mM HMF for six consecutive batches at 1.45 V vs. RHE.

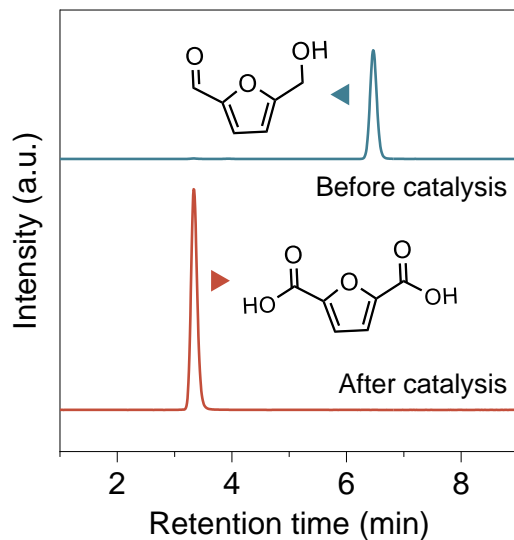


Fig. S15. The HPLC chromatograms of the solution before and after catalysis. It can be seen that all HMF is converted into FDCA.

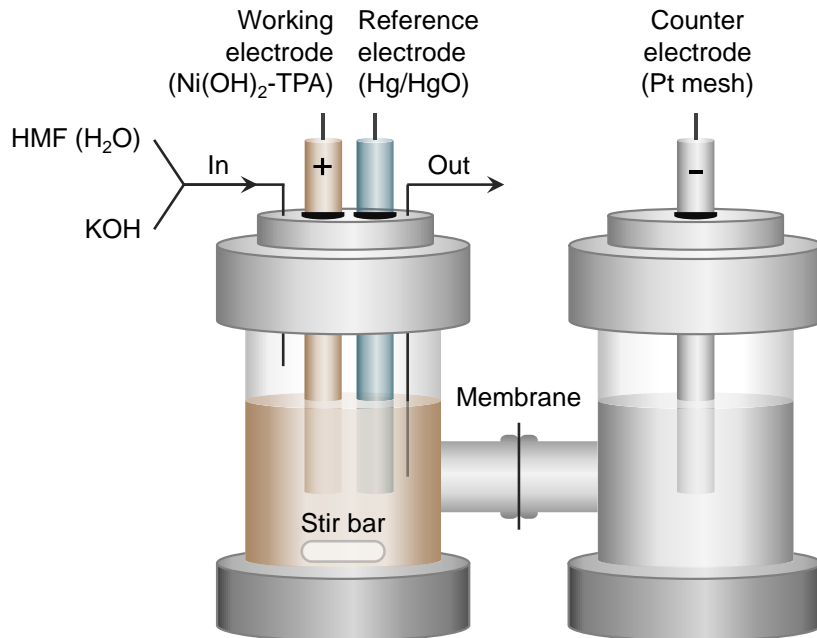


Fig. S16. Schematic illustration of H-type cell for CP test toward HMF oxidation.

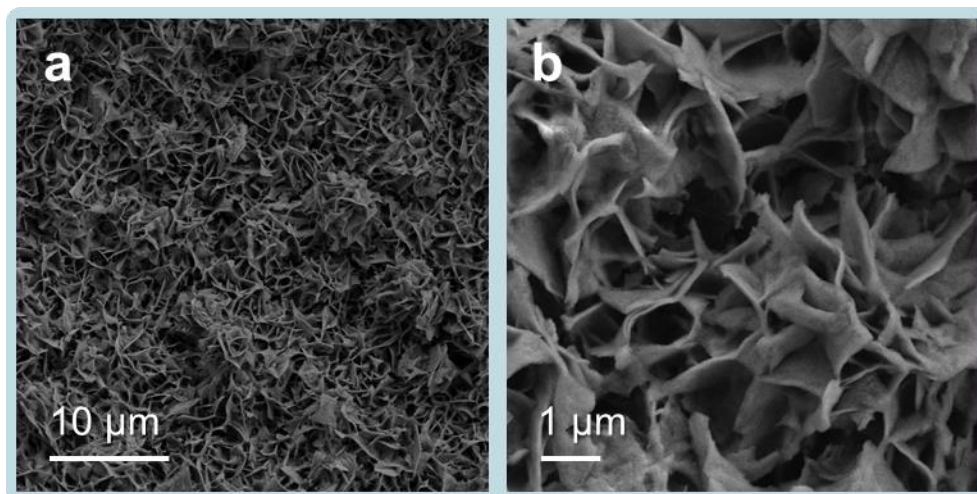


Fig. S17. SEM images with different magnifications of Ni(OH)₂-TPA after stability test.

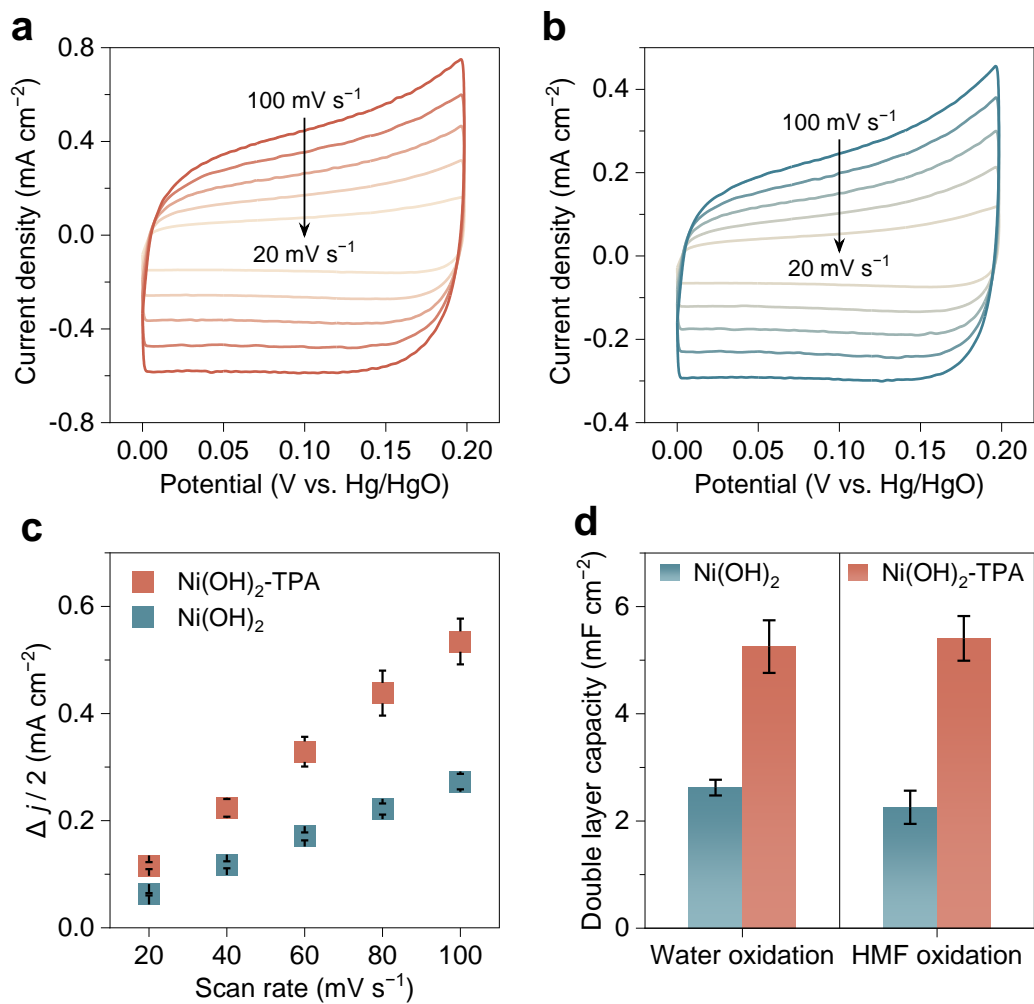


Fig. S18. Determination of ECSA. CV curves of (a) Ni(OH)₂-TPA and (b) Ni(OH)₂ at different scan rates (20, 40, 60, 80, and 100 mV s⁻¹) with 100 mM HMF. (c) Double layer charging current density ($\Delta j / 2$) plotted against scan rate with HMF. (d) Double layer capacity of catalysts for water oxidation and HMF oxidation.

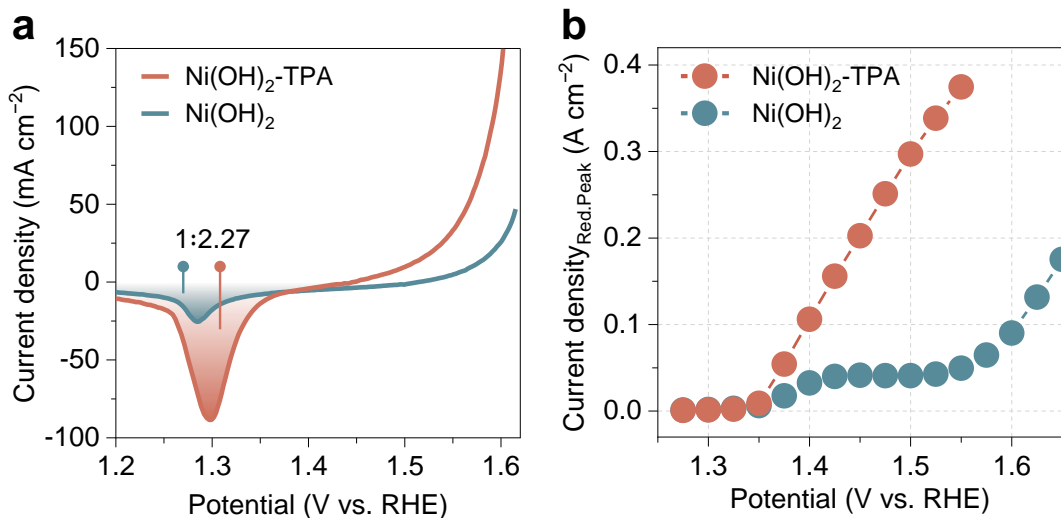


Fig. S19. (a) LSV plots (5 mV s^{-1}) of Ni(OH)₂-TPA and Ni(OH)₂ in 1.0 M KOH solution in reversal scan mode. The gradient color refers to the integration area of the reduction peak. (b) Reduction peak-normalized QS-LSV plots for HMFOR.

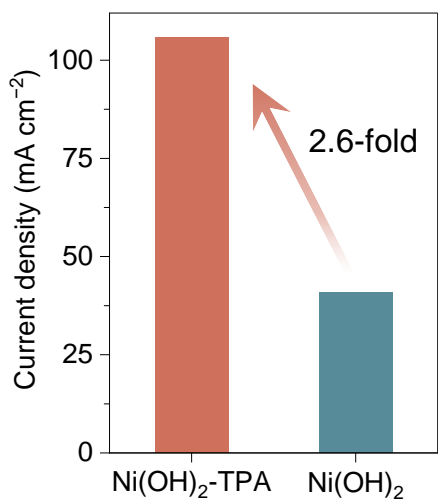


Fig. S20. Current density normalized through the ratio of charge passed (1:6.38 for Ni(OH)₂:Ni(OH)₂-TPA) at 1.50 V for HMF oxidation.

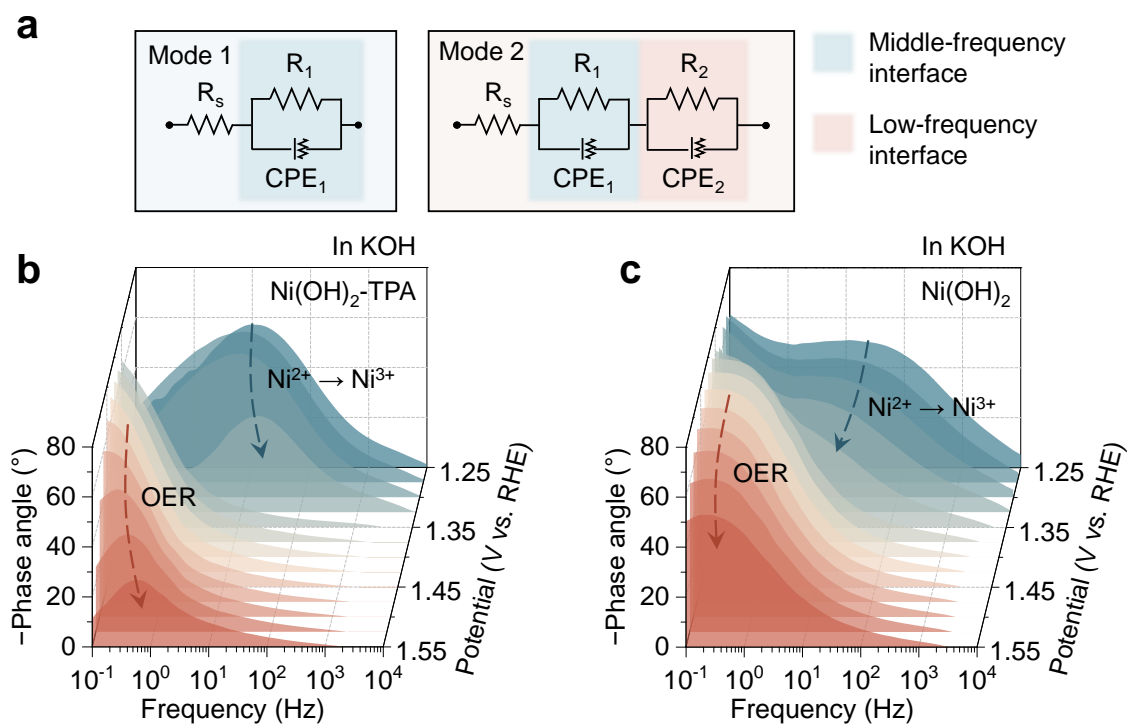


Fig. S21. (a) Two Modes for the fitted equivalent circuit. Operando EIS analysis for (b) Ni(OH)₂-TPA and (c) Ni(OH)₂ in 1.0 M KOH.

Note S2. The control operando EIS tests are performed in pure KOH solution to isolate the effect brought by HMF. As shown in **Fig. S21b** and **S21c**, the catalysts undergo electrooxidation ($\text{Ni}^{2+} \rightarrow \text{Ni}^{3+}$) under the strong oxidative potential in the middle-frequency region (10^0 – 10^2 Hz). With elevated potentials, the signals in the low-frequency region (10^{-1} – 10^0 Hz) refer to the nonhomogeneous charge distribution resulting from the surface oxidation for both catalysts. The low-frequency interface is hereby formed, where the OER occurs. The fitted equivalent circuit of these catalysts during OER follows Mode 2 in **Fig. S21a**. Despite that, the phase angle of Ni(OH)₂-TPA for OER is smaller than that of Ni(OH)₂, indicating that the charge at the catalyst/electrolyte interface prefers to participate in the Faradaic process instead of charge-discharge as a capacitor. TPA brings a fast interface reaction kinetics during the OER process. Even though, the current density of OER ($< 30 \text{ mA cm}^{-2}$) is still too low, the shift of the phase angle is mainly due to the intrinsic charge transfer inside the catalyst.

After introducing HMF, Ni(OH)₂-TPA exhibits a high reactivity and shows a high FE for FDCA. The fitted equivalent circuit follows Mode 1 in **Fig. S21a**. The difference lies in the vanish of the low-frequency interface, and that explains why only one signal can be observed in the middle-

frequency region (**Fig. 3e**). The high current density of HMFOR causes the fluctuation of signals. The significantly reduced phase angle verifies that TPA brings faster reaction kinetics, endowing the catalyst high specificity for HMFOR instead of OER. In contrast, Ni(OH)₂ mainly follows Mode 2 even with HMF (**Fig. 3f**), making OER the primary competition reaction. Thus, the signals are observable in the low-frequency region, and low FEs of FDCA also confirm it.

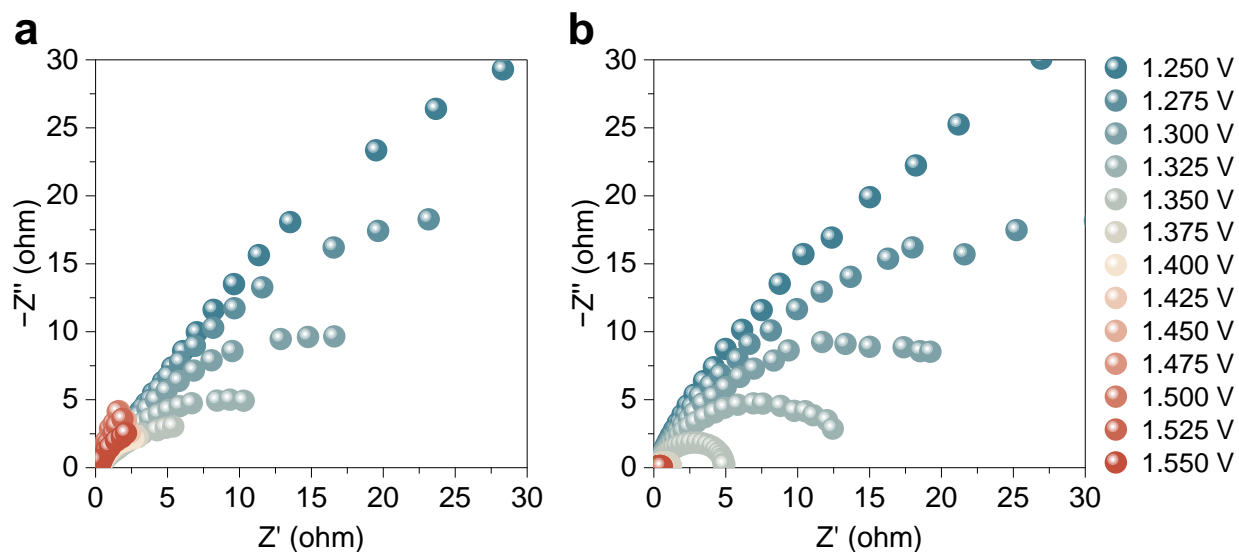


Fig. S22. Nyquist plots of (a) Ni(OH)₂ and (b) Ni(OH)₂-TPA for HMF oxidation (1.0 M KOH + 100 mM HMF) under increased potentials.

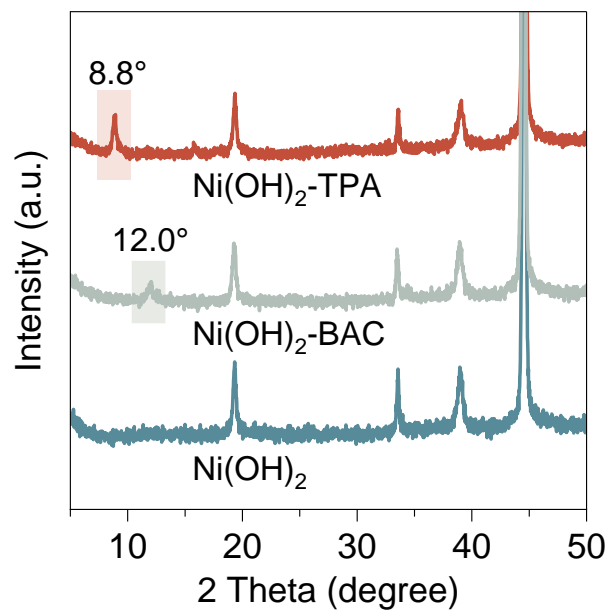


Fig. S23. XRD patterns of Ni(OH)₂-TPA, Ni(OH)₂-BAC, and Ni(OH)₂.

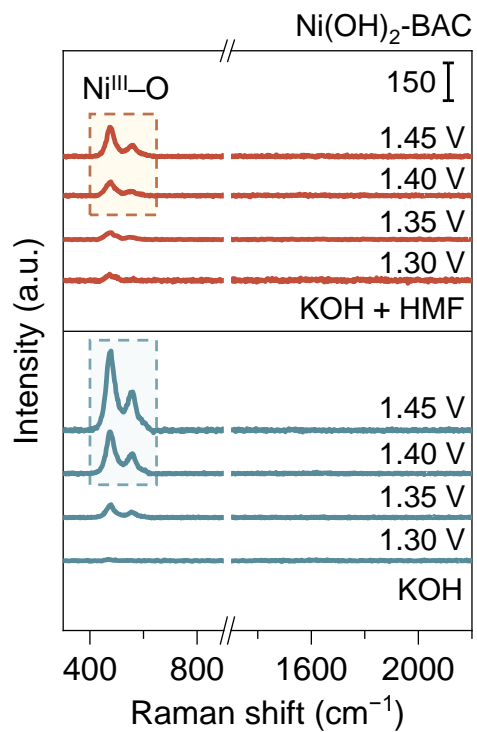


Fig. S24. Quasi-in-situ Raman spectra of Ni(OH)₂-BAC in KOH with and without HMF under elevating potentials.

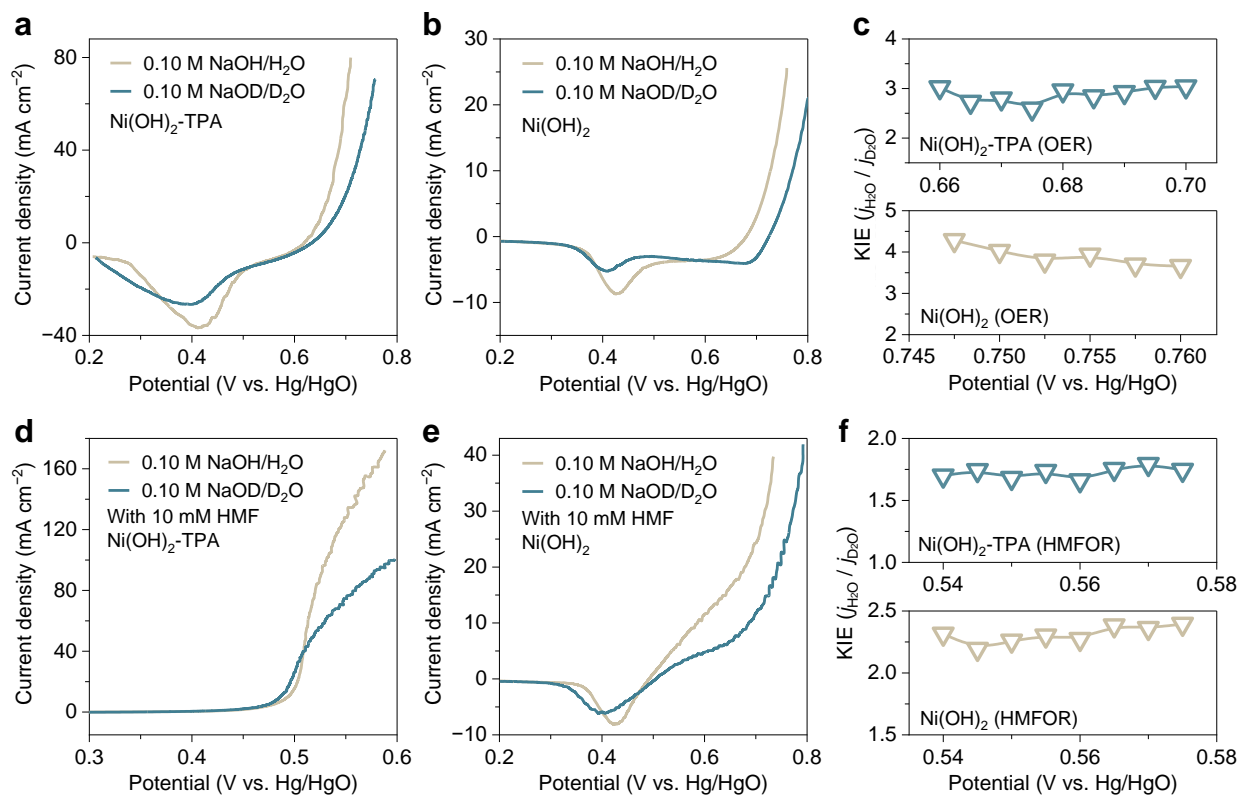


Fig. S25. LSV curves of (a) Ni(OH)₂-TPA and (b) Ni(OH)₂ in 0.10 M NaOH/H₂O and NaOD/D₂O, respectively. (c) Calculated KIE values for OER. LSV curves of (d) Ni(OH)₂-TPA and (e) Ni(OH)₂ in 0.10 M NaOH/H₂O and NaOD/D₂O in the presence of 10 mM HMF. (f) Calculated KIE values for HMFOR. Scan rate: 5 mV s⁻¹.

Note S3. The OER and HMFOR performances of Ni(OH)₂-TPA outperform pure Ni(OH)₂ in either NaOH/H₂O or NaOD/D₂O. For the OER process, the KIE values are calculated to be ~3.0 for Ni(OH)₂-TPA and ~3.7 for Ni(OH)₂ in the selected potential window, respectively. Both catalysts feature the primary KIEs (KIEs > 1.5), indicating that proton transfer is likely involved in the RDS or acts as a step that affects RDS during catalysis. The low KIE value of Ni(OH)₂-TPA specifies that O–H bond cleavage contributes to the RDS and shutting the generated proton by TPA ligand in this step helps accelerate the reaction kinetics.

After introducing HMF, all current densities intensify in the same potential window (**Fig. S25d** and **S25e**). As shown, the HMFOR activity of Ni(OH)₂-TPA is much greater than that of Ni(OH)₂. Ni(OH)₂-TPA reaches a KIE value of 1.75, which is lower than that of about 2.3 for Ni(OH)₂ during HMFOR. Thus, it can be concluded that Ni(OH)₂-TPA is less sensitive to the proton transfer process, which adequately confirms the significance of TPA in shuttling the proton generated during HMF oxidation.

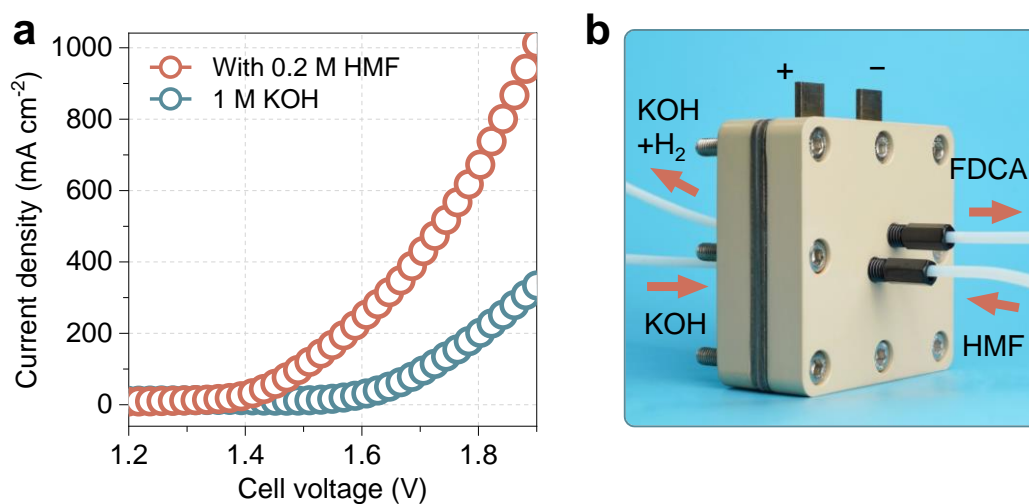


Fig. S26. (a) LSV plots of the Ni(OH)₂-TPA-based electrolyzer (1 cm²) with and without 0.2 M HMF (scan rate: 5 mV s⁻¹). (b) Optical photograph of the electrolyzer.

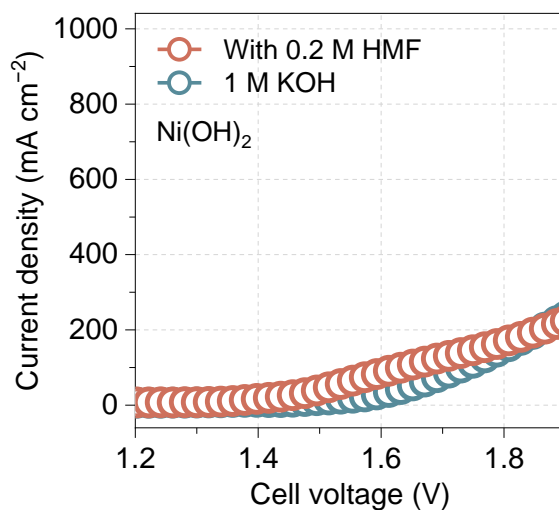


Fig. S27. LSV plots of the Ni(OH)₂-based electrolyzer (1 cm²) with and without 0.2 M HMF (scan rate: 5 mV s⁻¹).

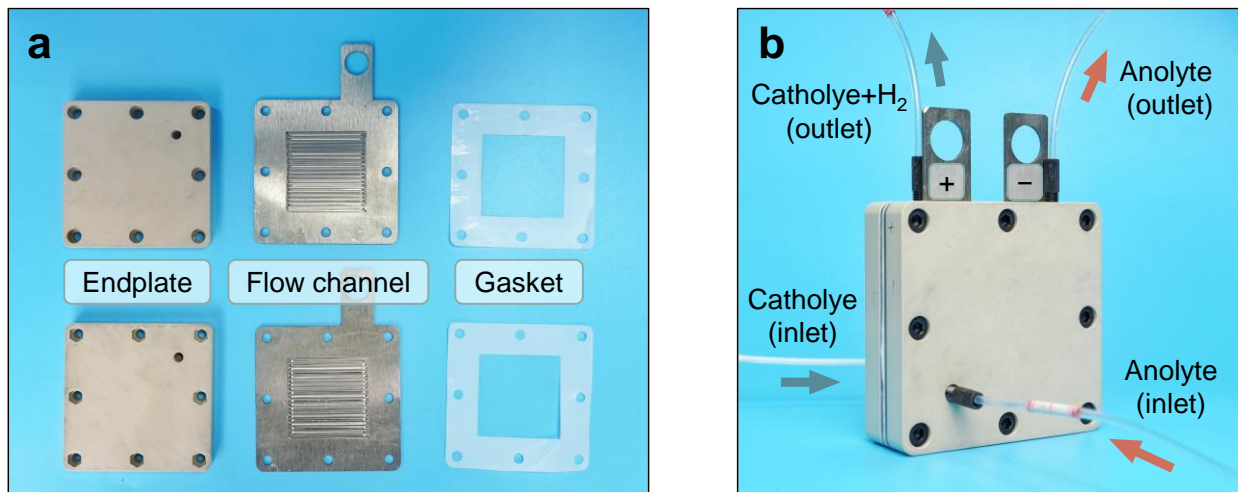


Fig. S28. (a) The structure of the AEM-HMFOR electrolyzer (25 cm²). (b) The flowing mode of the electrolyzer.

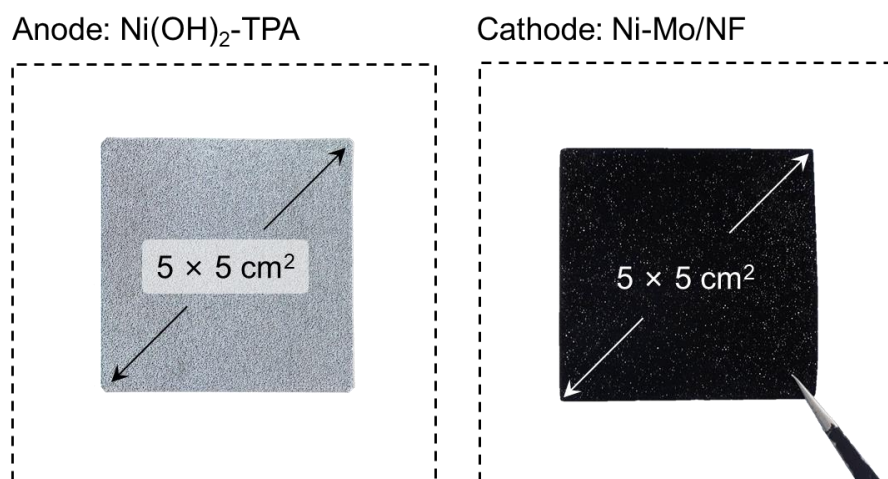


Fig. S29. Optical photograph of as-synthesized Ni(OH)₂-TPA and Ni-Mo/NF.

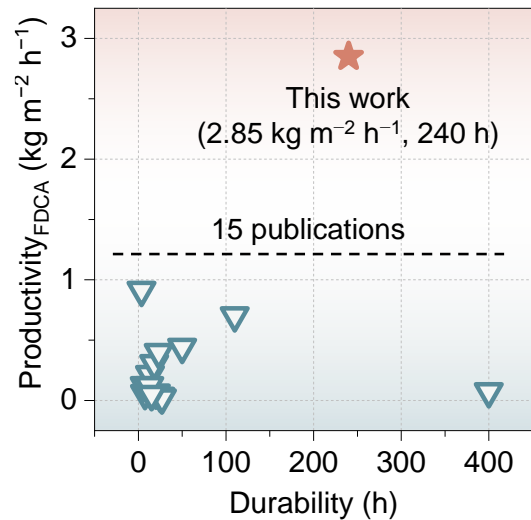


Fig. S30. Performance comparison of this work and 15 recent publications.

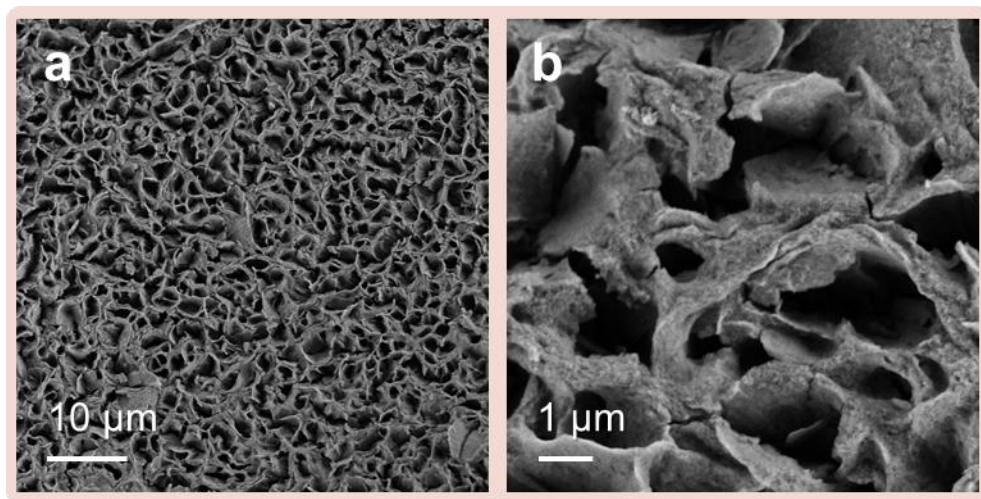


Fig. S31. SEM images with different magnifications of Ni(OH)₂-TPA after 240 hours stability test (7,500 mA) in an AEM-HMFOR electrolyzer.

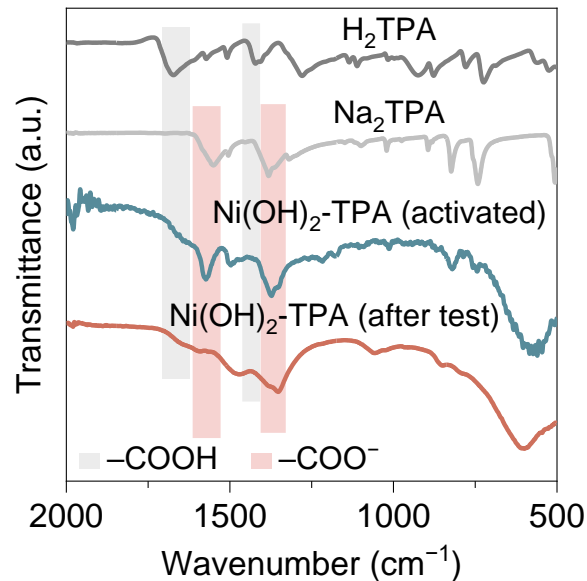


Fig. S32. FT-IR spectra of H₂TPA, Na₂TPA, Ni(OH)₂-TPA (activated through CV scans), and Ni(OH)₂-TPA (after test in AEM-HMFOR electrolyzer for 240 hours).

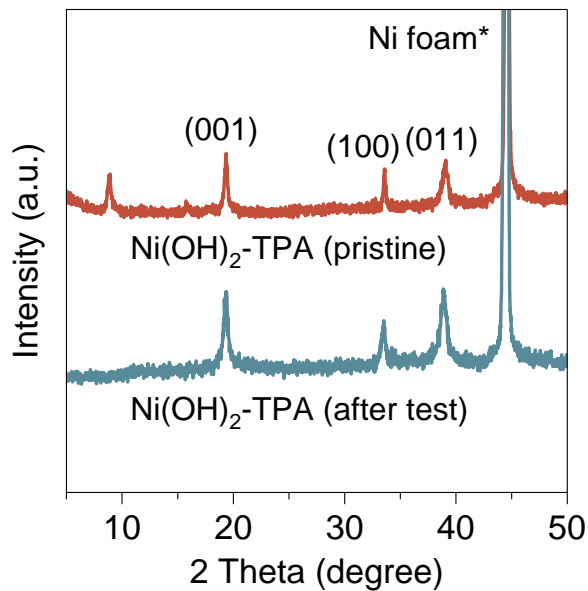


Fig. S33. XRD patterns of Ni(OH)₂-TPA before and after stability test for 240 h at a current of 7,500 mA. XRD test reveals that the Ni(OH)₂ skeleton remains unchanged after the test. Notably, the peak of the TPA intercalation vanished due to the break of the long-range order and the activation of the Ni(OH)₂-TPA catalyst.

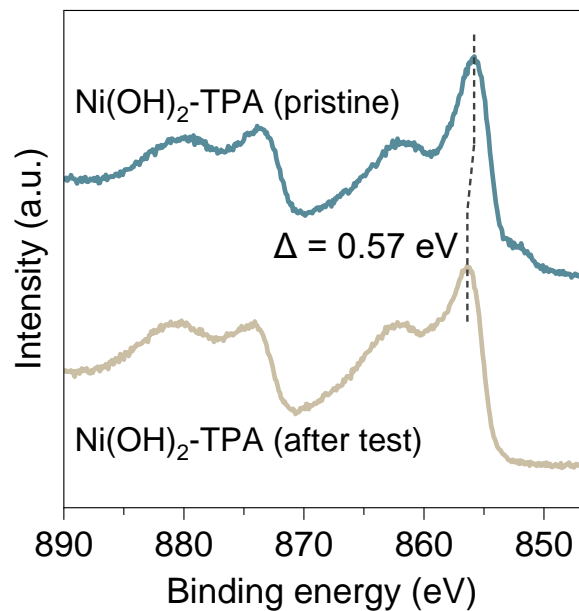


Fig. S34. XPS spectra of Ni(OH)₂-TPA before and after stability test.

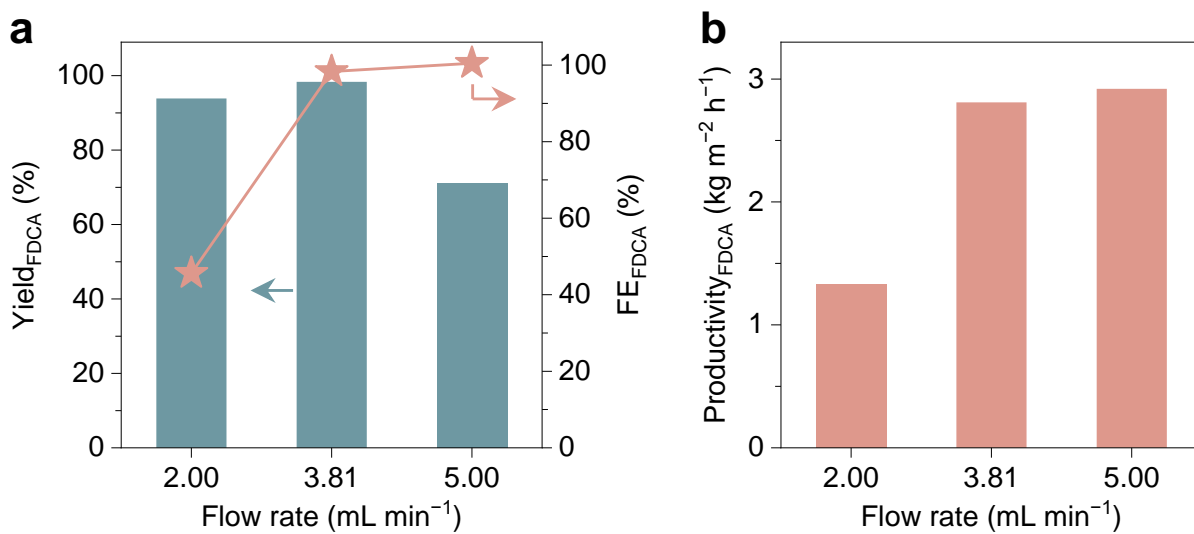


Fig. S35. (a) The evolution of yield and FE over flow rates in AEM-HMFOR electrolyzer (25 cm²). (b) The evolution of FDCA productivity at increased flow rates.

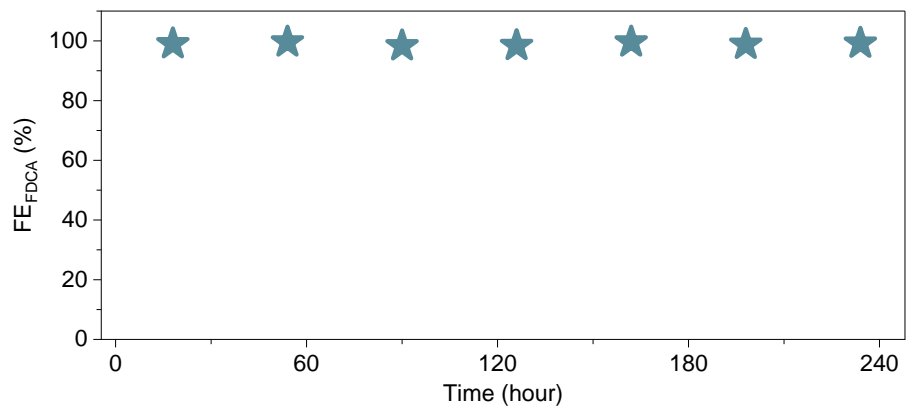


Fig. S36. Evolution of FEs of FDCA during stability measurement.

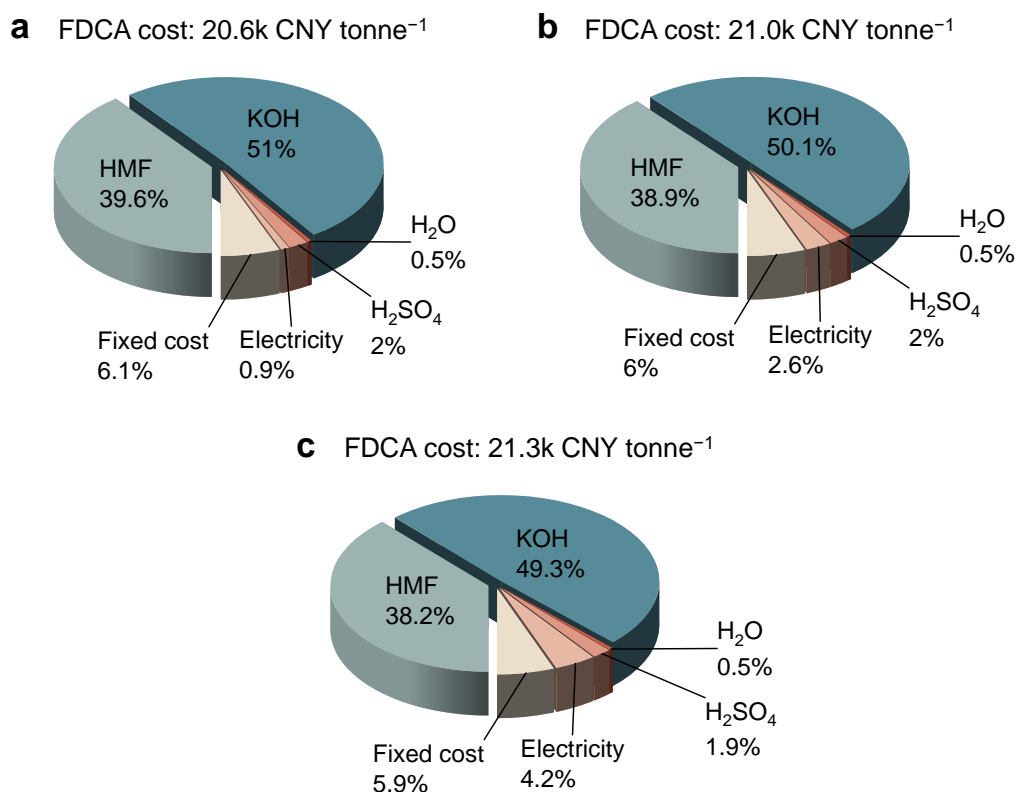


Fig. S37. Cost composition of FDCA when the electricity costs are (a) 0.10 CNY kWh⁻¹, (b) 0.30 CNY kWh⁻¹, and (c) 0.50 CNY kWh⁻¹ in 1.0 M KOH fed with 200 mM HMF.

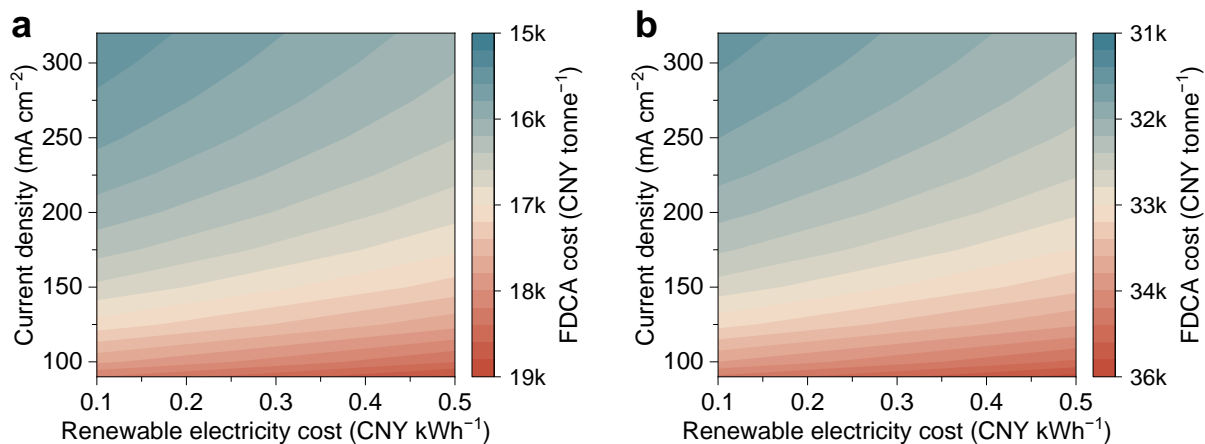
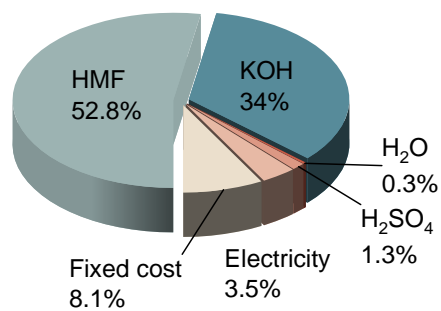


Fig. S38. Techno-economic analyses (TEA) for HMF oxidation electrolyzer fed with (a) 1.0 M KOH + 400 mM HMF and (b) 1.0 M KOH + 100 mM HMF.

Note S4. TEA for KOH (1.0 M) with different HMF concentrations (100, 200, 400 mM) is analyzed. As is known, the production of 1 molecule FDCA requires 1 molecule HMF and 2 molecule KOH. Thus, the concentration of KOH is generally 2 times higher than HMF. In 1.0 M KOH with 100 mM HMF, when the equivalent reaction is completed, there is still 0.8 M KOH unreacted. And the concentration of FDCA remains low (100 mM). Most of the unreacted KOH is neutralized by H_2SO_4 , leading to an increase in material cost. However, when HMF concentration reaches 400 mM, even if the same amount of H_2SO_4 is required to neutralize KOH and acidize FDCA (in the form of K^+ salt), the high concentration of FDCA helps reduce the material cost (particularly for KOH), resulting in the much lower FDCA production cost. Therefore, in the future design of AEM-based HMFOR electrolyzers, the HMF concentration needs to be seriously considered, which may significantly influence the final prize of FDCA and a more industrial-relevant HMF concentration (at least > 200 mM) shall be further explored.

a FDCA cost: 15.5k CNY tonne⁻¹



b FDCA cost: 32.0k CNY tonne⁻¹

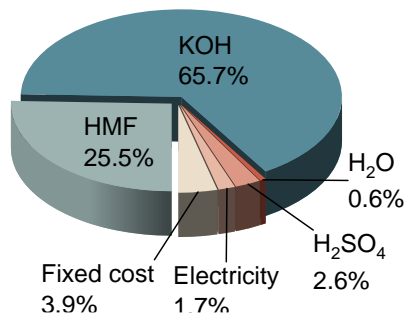


Fig. S39. Cost composition of FDCA in 1.0 M KOH fed with (a) 400 mM HMF and (b) 100 mM HMF at an electricity cost of 0.30 CNY kWh⁻¹.

Table S1 Comparison of the performance of HMF electrooxidation systems.

Productivity (kg h ⁻¹ m ⁻²)	Time (hour)	Electrocatalysts	Reference
0.70	110	NiCoB _x	<i>Chem</i> , 2024, 10 , 2147–2169
0.06	7.5	Ag–Co(OH) ₂	<i>Adv. Mater.</i> , 2024, 36 , 2312402
0.22	13.3	NiCo PBA	<i>ACS Catal.</i> , 2024, 14 , 9565–9574
0.05	15	NiS _x /β-Ni(OH) ₂ /Ni	<i>Adv. Mater.</i> , 2023, 35 , 2211177
0.07	400	Ni(OH) ₂ /Cu(OH) ₂	<i>Energy Environ. Sci.</i> , 2024, 17 , 8801–8809
0.44	50	CoOOH/NF	<i>Nat. Commun.</i> , 2023, 14 , 5621
0.12	7.315	Co-NiC ₂ O ₄ /NF	<i>J. Am. Chem. Soc.</i> , 2023, 145 , 20624–20633
0.03	25	InOOH-OV	<i>Nat. Commun.</i> , 2023, 14 , 2040
0.31	18	NiCo LDH	<i>Energy Environ. Sci.</i> , 2023, 16 , 5305–5314
0.06	20	Cu ₂ P ₇ -CoP	<i>Chem. Eur. J.</i> , 2023, 29 , e202300973
0.02	26.9	NF@Co ₃ O ₄ /CeO ₂	<i>Adv. Funct. Mater.</i> , 2023, 33 , 2213170
0.91	3.6	Cr-Ni(OH) ₂ /NF	<i>Appl. Catal., B.</i> , 2023, 330 , 122950
0.40	23.3	NiCoFeS-MOF	<i>J. Mater. Chem. A</i> , 2023, 11 , 6375–6383
0.12	12.5	Ni-Co ₂ P	<i>Nano Res.</i> , 2023, 16 , 6728–6735
0.05	15	Co ₃ O ₄ /NF	<i>J. Colloid Interface Sci.</i> , 2023, 632 , 87–94
2.85	240	Ni(OH)₂-TPA	This work